J|A|C|S ARTICLES

Published on Web 10/28/2009

Structural Phase Transitions and Superconductivity in $Fe_{1+\delta}Se_{0.57}Te_{0.43}$ at Ambient and Elevated Pressures

Nathalie C. Gresty,[†] Yasuhiro Takabayashi,[†] Alexey Y. Ganin,[‡] Martin T. McDonald,[†] John B. Claridge,[‡] Duong Giap,[‡] Yoshikazu Mizuguchi,[§] Yoshihiko Takano,[§] Tomoko Kagayama,[||] Yasuo Ohishi,[⊥] Masaki Takata,[⊥] Matthew J. Rosseinsky,*[,‡] Serena Margadonna,*[,○] and Kosmas Prassides*[,†]

Department of Chemistry, Durham University, Durham DH1 3LE, U.K., Department of Chemistry, University of Liverpool, Liverpool L69 7ZD, U.K., National Institute for Materials Science, 1-2-1 Sengen, Tsukuba 305-0047, Japan, Center for Quantum Science and Technology under Extreme Conditions, Osaka University, Osaka 560-8531, Japan, Japan Synchrotron Radiation Research Institute, SPring-8, Hyogo 679-5198, Japan, and School of Chemistry, University of Edinburgh, Edinburgh EH9 3JJ, U.K.

Received August 31, 2009; E-mail: m.j.rosseinsky@liverpool.ac.uk; serena.margadonna@ed.ac.uk; K.Prassides@durham.ac.uk

Abstract: The ternary iron chalcogenide, $Fe_{1.03}Se_{0.57}Te_{0.43}$ is a member of the recently discovered family of Fe-based superconductors with an ambient pressure T_c of 13.9 K and a simple structure comprising layers of edge-sharing distorted $Fe(Se/Te)_4$ tetrahedra separated by a van der Waals gap. Here we study the relationship between its structural and electronic responses to the application of pressure. T_c depends sensitively on applied pressure attaining a broad maximum of 23.3 K at ~3 GPa. Further compression to 12 GPa leads to a metallic but nonsuperconducting ground state. High-resolution synchrotron X-ray diffraction shows that the superconducting phase is metrically orthorhombic at ambient pressure but pressurization to ~3 GPa leads to a structural transformation to a more distorted structure with monoclinic symmetry. The exact coincidence of the crystal symmetry crossover pressure with that at which T_c is maximum reveals an intimate link between crystal and electronic structures of the iron chalcogenide superconductors.

Introduction

The iron chalcogenides, FeQ (Q = Se, Te), with the layered anti-PbO tetragonal structure at ambient temperature are parent members of the recently discovered Fe-based high-T_c superconductors.[1−3] They possess FeQ slabs of edge-sharing FeQ_4 tetrahedra isostructural and isoelectronic to those of the $(FePn)^-$ (Pn = As, P) families, and they have comparable 2D electronic structures.[4] In addition, they are structurally the simplest currently available members as there are no guest ions (*cf.* LiFeAs; $AEFe_2As_2$, AE = alkaline earth)[5,6] or interleaved slabs (*cf.* REFeAsO, RE = rare earth; AEFeAsF)[1,2,7] in the interlayer van der Waals gap. α-FeSe is superconducting at ambient P with $T_c \approx 8$ K.[3] Its electronic behavior is very sensitive to disorder and defects, and superconductivity appears to occur over a limited range of $Fe_{1+\delta}Se$ ($\delta \approx 0.01$) nonstoichiometry.[8] Its low-temperature crystal structure in the superconducting state is orthorhombic (space group *Cmma*),[9] identical to those of the undoped parent materials[10] and underdoped superconducting members[11] of the $REFeAsO_{1-x}F_x$ (RE = rare earth, $x < 0.15$) families. No long-range magnetic order is present[12,13] although

[†] Durham University.
[‡] University of Liverpool.
[§] National Institute for Materials Science.
[||] Osaka University.
[⊥] SPring-8.
[○] University of Edinburgh.

(1) Kamihara, Y.; Watanabe, T.; Hirano, M.; Hosono, H. *J. Am. Chem. Soc.* **2008**, *130*, 3296.
(2) Chen, X. H.; Wu, T.; Wu, G.; Liu, R. H.; Chen, H.; Fang, D. F. *Nature* **2008**, *453*, 761.
(3) Hsu, F.-C.; Luo, J.-Y.; Yeh, K.-W.; Chen, T.-K.; Huang, T.-W.; Wu, P. M.; Lee, Y.-C.; Huang, Y.-L.; Chu, Y.-Y.; Yan, D.-C.; Wu, M.-K. *Proc. Natl. Acad. Sci. U.S.A.* **2008**, *105*, 14262.
(4) Subedi, A. *Phys. Rev. B* **2008**, *78*, 134514.
(5) (a) Pitcher, M. J.; Parker, D. R.; Adamson, P.; Herkelrath, S. J. C.; Boothroyd, A. T.; Ibberson, R. M.; Brunelli, M.; Clarke, S. J. *Chem. Commun.* **2008**, 5918. (b) Tapp, J. H.; Tang, Z.; Lv, B.; Sasmal, K.; Lorenz, B.; Chu, P. C. W.; Guloy, A. M. *Phys. Rev. B* **2008**, *78*, 060505(R).
(6) (a) Rotter, M.; Tegel, M.; Johrendt, D. *Phys. Rev. Lett.* **2008**, *101*, 107006. (b) Sasmal, K.; Lv, B.; Lorenz, B.; Gouloy, A. M.; Chen, F.; Xue, Y.; Chu, P. C. W. *Phys. Rev. Lett.* **2008**, *101*, 107007.
(7) Matsuishi, S.; Inoue, Y.; Nomura, T.; Yanagi, H.; Hirano, M.; Hosono, H. *J. Am. Chem. Soc.* **2008**, *130*, 14428.
(8) McQueen, T. M.; Huang, Q.; Ksenofontov, V.; Felser, C.; Xu, Q.; Zandbergen, H. W.; Hor, Y. S.; Allred, J.; Williams, A. J.; Qu, D.; Checkelsky, J.; Ong, N. P.; Cava, R. J. *Phys. Rev. B* **2009**, *79*, 014522.
(9) Margadonna, S.; Takabayashi, Y.; McDonald, M. T.; Kasperkiewicz, K.; Mizuguchi, Y.; Takano, Y.; Fitch, A. N.; Suard, E.; Prassides, K. *Chem. Commun.* **2008**, 5607.
(10) (a) Nomura, T.; Kim, S. W.; Kamihara, Y.; Hirano, M.; Sushko, P. V.; Kato, K.; Takata, M.; Shluger, A. L.; Hosono, H. *Supercond. Sci. Technol.* **2008**, *21*, 125028. (b) de la Cruz, C.; Huang, Q.; Lynn, J. W.; Li, J.; Ratcliff, W.; Zarestky, J. L.; Mook, H. A.; Chen, G. F.; Luo, J. L.; Wang, N. L.; Dai, P. *Nature* **2008**, *453*, 899.
(11) Margadonna, S.; Takabayashi, Y.; McDonald, M. T.; Brunelli, M.; Wu, G.; Liu, R. H.; Chen, X. H.; Prassides, K. *Phys. Rev. B* **2009**, *79*, 014503.
(12) Kotegawa, H.; Masaki, S.; Awai, Y.; Tou, H.; Mizuguchi, Y.; Takano, Y. *J. Phys. Soc. Jpn.* **2008**, *77*, 113703.

 10.1021/ja907345x CCC: $40.75

there is some evidence that spin fluctuations are present above T_c.[13] Moreover, the response of the superconducting transition of α-FeSe to applied pressure is complex. The initial pressure coefficient, dT_c/dP, is very large and positive (~9.1 K GPa^{-1}), and T_c rises rapidly to 27 K at 1.48 GPa.[14] A further increase in pressure leads to the attainment of a broad maximum of 37 K at ~7 GPa, one of the highest T_c reported for a binary solid.[15,16] At higher pressures, dT_c/dP becomes negative and T_c is rapidly suppressed. The nonmonotonic $T_c(P)$ behavior is mirrored by accompanying drastic anomalies in the pressure evolution of the interlayer spacing of the highly anisotropic crystal structure. At the same time, there is a pressure-induced phase transition of the PbO-type FeSe structure to that of the more densely packed nonsuperconducting β-polymorph near 9 GPa.

On the other hand, neither of the isostructural FeS and FeTe solids has been found to be superconducting. In particular, the α-$Fe_{1+\delta}Te$ binary orders antiferromagnetically at low temperatures and can accommodate significant amounts of excess Fe ($\delta \leq 0.14$), which leads to different lattice distortions of the room-temperature tetragonal structure on cooling.[17,18] For instance, the low-temperature crystal structures of $Fe_{1.08}Te$ and $Fe_{1.14}Te$ phases are monoclinic (space group $P2_1/m$) and orthorhombic (*Pmmn*), respectively. Attempts to induce superconductivity by the application of pressure to the α-$Fe_{1+\delta}Te$ system have been so far unsuccessful.[19] However, superconductivity survives in the $Fe_{1+\delta}Se_{1-x}Q_x$ (Q = Te, S) phase field for a broad range of nominal values of the dopant level x, and the ambient pressure T_c maximizes at ~15 K for the composition with nominal stoichiometry $FeSe_{0.5}Te_{0.5}$.[20]

In an attempt to obtain a detailed understanding of the structure of the ternary α-$Fe_{1+\delta}Se_{1-x}Te_x$ phases and the implications for superconductivity, we have undertaken a systematic high-resolution synchrotron X-ray diffraction study at ambient and elevated pressures combined with high-pressure magnetization and resistance measurements for the phase with nominal stoichiometry $FeSe_{0.5}Te_{0.5}$ (T_c = 13.9 K at ambient P). We find that, at ambient pressure and low temperatures, the structure is orthorhombic (space group *Cmma*), isostructural with α-FeSe,[9] and incorporates a small amount of Fe defects ($\delta \approx 0.03$). The initial pressure coefficient, dT_c/dP, is large and positive with T_c rapidly increasing with applied pressure to 23 K at ~3 GPa. Further compression leads to a rapid decrease in T_c, and the sample is metallic but not superconducting at ~12 GPa. Unlike the α-FeSe polymorph, we find that the present system remains structurally robust to applied pressures as high as 10 GPa; however, its low-temperature crystal structure becomes metrically monoclinic exactly in the same pressure range where the maximum in $T_c(P)$ occurs, thereby implying that the crystal symmetry of the low-temperature structure plays a key role in defining the electronic properties of the iron chalcogenide superconductors.

Experimental Details

A polycrystalline sample with nominal composition $FeSe_{0.5}Te_{0.5}$ was synthesized by a conventional solid state reaction. In a He-filled glovebox, 56.3 mg (0.721 mmol) of Se (Alfa Aesar, 99.999%), 92.0 mg (0.721 mmol) of Te (Alfa Aesar, 99.999%), and 80.5 mg (1.442 mmol) of Fe (Alfa Aesar, 99.999%) were loaded into an 8-mm silica ampule, which was sealed under a dynamic vacuum (<10^{-5} Torr). The ampule was heated from ambient temperature to 680 °C at 30 °C/h, and after 48 h of reaction time it was cooled at 120 °C/h to ambient temperature. The product was reground in the glovebox, resealed in a silica ampule, and heated following the same reaction protocol described above. The procedure was repeated once more. All measurements in this work were performed on the same sample batch.

The sample was characterized by powder X-ray diffraction and temperature-dependent dc magnetization measurements at ambient P. Bulk superconductivity is observed at 13.9 K. Magnetization measurements were carried out at 20 Oe on a ~20-mg sample in the temperature range 1.8−30 K under both zero-field-cooling (ZFC) and field-cooling (FC) protocols with a Quantum Design SQUID magnetometer. Hydrostatic external pressure to ~1.02 GPa was applied with a piston-cylinder high-pressure cell (easyLab Technologies Mcell10) using high-purity Sn as an *in situ* manometer. The error in the pressure determination is ~0.02 GPa. Daphne mineral oil was used as the pressure transmitting medium. Magnetization data were collected on both increasing and decreasing P. Electrical resistance measurements under high pressures (to ~12 GPa) were performed by a standard four-probe technique using a diamond anvil cell (DAC). The diameter of the diamond culet was 500 μm, and the sample was introduced in a hole made in a rhenium gasket 90 μm deep and 180 μm in diameter. The top surface of the gasket was coated with a c-BN layer to provide electrical isolation between the electrodes and the metal part. Powdered NaCl was used as a pressure-transmitting medium. Pressure was applied at 100 K and measured by the ruby fluorescence method at low temperature. These values are used to discuss the pressure dependence of T_c. Resistance data were collected on both increasing and decreasing P.

High-resolution synchrotron X-ray diffraction experiments were carried out on the ID31 beamline at the European Synchrotron Radiation Facility (ESRF), France. The sample was sealed in a 1-mm diameter thin-wall glass capillary, and diffraction profiles (λ = 0.399 88 Å) were collected in continuous scanning mode at various temperatures between 5 and 295 K. The data were rebinned in the 2θ range 1°−30° to a step of 0.001°. Higher statistic diffraction profiles were also recorded at 5, 100, 200, and 295 K over a wider angular range (2θ = 1°−50°). Analysis of the diffraction data was performed with the GSAS suite of Rietveld programs.[21] High-pressure synchrotron X-ray diffraction experiments at 14 K were performed at beamline BL10XU, SPring-8, Japan. The powdered sample was loaded in a helium-gas-driven membrane diamond anvil cell (MDAC), which was equipped with a Be−Cu alloy gasket and placed inside a closed-cycle helium refrigerator. The diameter of the diamond culet was 600 μm, and

(13) Imai, T.; Ahilan, K.; Ning, F. L.; McQueen, T. M.; Cava, R. J. *Phys. Rev. Lett.* **2009**, *102*, 177005.
(14) Mizuguchi, Y.; Tomioka, F.; Tsuda, S.; Yamaguchi, T.; Takano, Y. *Appl. Phys. Lett.* **2008**, *93*, 152505.
(15) Margadonna, S.; Takabayashi, Y.; Ohishi, Y.; Mizuguchi, Y.; Takano, Y.; Kagayama, T.; Nakagawa, T.; Takata, M.; Prassides, K. *Phys. Rev. B* **2009**, *80*, 064506.
(16) Medvedev, S.; McQueen, T. M.; Trojan, I.; Palasyuk, T.; Eremets, M. I.; Cava, R. J.; Naghavi, S.; Casper, F.; Ksenofontov, V.; Wortmann, G.; Felser, C. *Nat. Mater.* **2009**, *8*, 630.
(17) Li, S.; de la Cruz, C.; Huang, Q.; Chen, Y.; Lynn, J. W.; Hu, J.; Huang, Y. L.; Hsu, F. C.; Yeh, K. W.; Wu, M. K.; Dai, P. *Phys. Rev. B* **2009**, *79*, 054503.
(18) Bao, W.; Qiu, Y.; Huang, Q.; Green, M. A.; Zajdel, P.; Fitzsimmons, M. R.; Zhernenkov, M.; Fang, M.; Qian, B.; Vehstedt, E. K.; Yang, J.; Pham, H. M.; Spinu, L.; Mao, Z. Q. *Phys. Rev. Lett.* **2009**, *102*, 247001.
(19) Okada, H.; Takahashi, H.; Mizuguchi, Y.; Takano, Y.; Takahashi, H. *J. Phys. Soc. Jpn.* **2009**, *78*, 083709.
(20) (a) Yeh, K. W.; Huang, T. W.; Huang, Y. L.; Chen, T. K.; Hsu, F. C.; Wu, P. M.; Lee, Y. C.; Chu, Y. Y.; Chen, C. L.; Luo, J. Y.; Yan, D. C.; Wu, M. K. *Europhys. Lett.* **2008**, *84*, 37002. (b) Fang, M. H.; Pham, H. M.; Qian, B.; Liu, T. J.; Vehstedt, E. K.; Liu, Y.; Spinu, L.; Miao, Z. Q. *Phys. Rev. B* **2008**, *78*, 224503. (c) Mizuguchi, Y.; Tomioka, F.; Tsuda, S.; Yamaguchi, T.; Takano, Y. *Appl. Phys. Lett.* **2009**, *94*, 012503.
(21) Larsen, A. C.; von Dreele, R. B. GSAS software, Los Alamos National Laboratory Report No. LAUR 86-748.

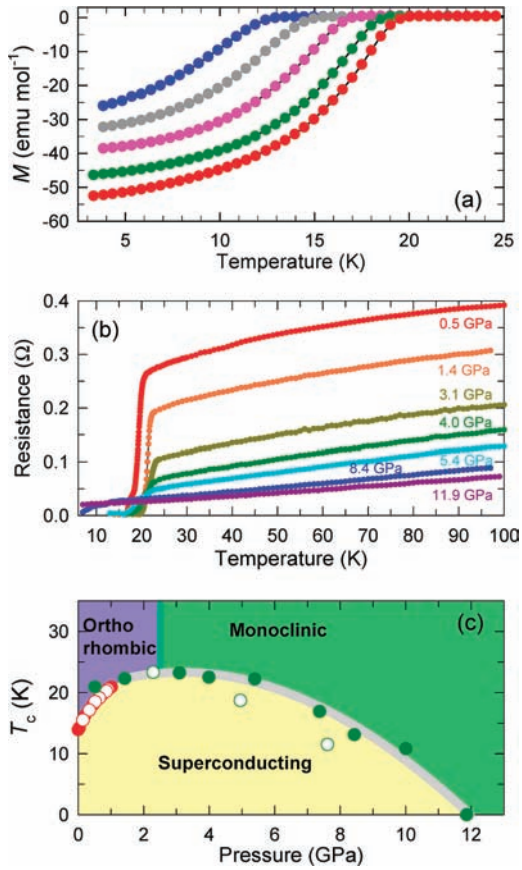

Figure 1. (a) Temperature dependence of the magnetization, M (ZFC, 20 Oe), at 0.04, 0.20, 0.46, 0.71, and 1.02 GPa (from left to right) for α-$Fe_{1.03}Se_{0.57}Te_{0.43}$. (b) Temperature dependence of the resistance, R, at selected pressures up to 11.9 GPa. (c) Pressure evolution of T_c obtained from the magnetization (full red circles, increasing P; open red circles, decreasing P; T_c is defined as the temperature at which M begins to decrease) and resistivity (full green circles, increasing P; open green circles, decreasing P; T_c is defined as the temperature at which R begins to decrease) measurements as a function of applied pressure.

the sample was introduced in a hole made in the gasket 150 μm deep and 600 μm in diameter. Daphne mineral oil loaded in the MDAC was used as a pressure medium. The applied pressure was increased at 14 K by controlling the He gas pressure on the MDAC diaphragm without dismounting the cell from the cryostat and was measured with the ruby fluorescence method. The diffraction patterns (λ = 0.411 18 Å) were collected using a flat image plate detector (Rigaku R-AXIS IV++, 300 × 300 mm^2 area and 0.100 mm pixel size) up to a maximum pressure of ~10 GPa. Masking of the strong Bragg reflections of the diamond anvil and integration of the two-dimensional diffraction images were performed with the WinPIP software. Data analysis of the resulting one-dimensional diffraction profiles was also performed with the GSAS suite of Rietveld programs.

Results

Magnetization and Resistance Measurements at High *P*. Figure 1a shows the temperature dependence of the ZFC magnetization, M, at various pressures for the sample with nominal composition $FeSe_{0.5}Te_{0.5}$. Close to ambient P, bulk superconductivity with an onset T_c of 14.2 K and a shielding fraction of 32% (at 3.8 K) is observed. The superconducting response to increasing P is very sensitive; T_c shifts to higher temperatures (at an initial rate of ~10 K GPa^{-1}) with a distinct parabolic curvature at higher P and reaches a maximum value of 20.9 K at 1.02 GPa (Figure 1c). No broadening of the transition is observed with increasing P implying the absence of sample inhomogeneities, while the shielding fraction approaches 64% at 1.02 GPa (Figure 1S).

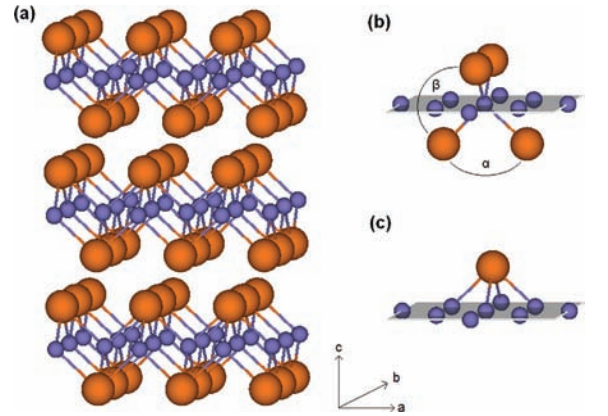

Figure 2. (a) Schematic diagram of the crystal structure of α-$Fe_{1.03}Se_{0.57}Te_{0.43}$. Fe and Se/Te ions are depicted as blue and brown spheres, respectively. The Fe defect is omitted for clarity. Geometry of the (b) $Fe(Se/Te)_4$ tetrahedra and (c) the $(Se/Te)Fe_4$ pyramids. In (b), α and β label the two symmetry-inequivalent Se/Te−Fe−Se/Te angles bisected by the c axis and the ab plane, respectively.

The temperature dependence of the resistance of the same $FeSe_{0.5}Te_{0.5}$ sample at various pressures up to 11.9 GPa is shown in Figure 1b. The onset T_c at the lowest measured pressure of 0.5 GPa is 20.9 K with the zero resistance state reached at 16.8 K in good agreement with the magnetization data. However, the data show a distinct step at intermediate temperatures (Figure 2S) that is usually associated with the presence of a second superconducting phase. This resistance step is very sensitive to the applied current during the measurements. Given that no evidence for a comparable effect is found in the magnetization data (Figure 1a), that the minority hexagonal NiAs-structured polymorph present is nonsuperconducting over the pressure range studied, and that high-resolution synchrotron XRD unambiguously shows the absence of phase separation (*vide infra*), we attribute the observed response to grain boundary effects. All subsequent $R(T)$ data sets were measured with a current of 10 μA. As pressure increases above 0.5 GPa, T_c increases further and reaches a maximum of 23.2 K at 3.1 GPa (Figure 1b). At higher pressures, the pressure coefficient of T_c becomes negative and T_c is rapidly suppressed to 10.8 K at 10 GPa. Further increase in P to 11.9 GPa leads to the disappearance of superconductivity. However, R continues to decrease monotonically with decreasing temperature, implying that the $FeSe_{0.5}Te_{0.5}$ sample remains metallic to the highest pressure of the present measurements. Pressure release led to the recovery of the superconducting response. The relation between T_c and pressure for $FeSe_{0.5}Te_{0.5}$ is summarized in Figure 1c, which clearly shows that the change in sign of the pressure coefficient, dT_c/dP, occurs for pressures between 2.3 and 3.1 GPa. These results are in good agreement with those reported in ref 22 where a maximum in T_c at 26 K was found near 2 GPa for a sample with nominal composition $FeSe_{0.5}Te_{0.5}$.

Structural Response of α-$Fe_{1.03}Se_{0.57}Te_{0.43}$ to Temperature at Ambient Pressure. Inspection of the synchrotron X-ray diffraction profile of the sample at 295 K confirmed the primitive tetragonal (T) unit cell (a_T = 3.800742(4) Å, c_T = 5.99263(3)

(22) Horigane, K.; Takeshita, N.; Lee, C.-H.; Hiraka, H.; Yamada, K. *J. Phys. Soc. Jpn.* **2009**, *78*, 063705.

Table 1. Refined Structural Parameters and Selected Bond Lengths (Å) and Angles (deg) for α-$Fe_{1.03}Se_{0.57}Te_{0.43}$ Obtained from Rietveld Refinements of the Synchrotron X-ray Powder Diffraction Data at Selected Temperatures and Pressures[a]

Temperature		295 K	5 K	14 K	14 K	14 K
Pressure		Ambient	Ambient	0.2 GPa	4.0 GPa	9.8 GPa
Space group		*P4/nmm*	*Cmma*	*Cmma*	$P2_1/m$	$P2_1/m$
a (Å)		3.800742(4)	5.37501(3)	5.3590(2)	3.7059(2)	3.6460(4)
b (Å)			5.36526(3)	5.3453(3)	3.6939(3)	3.6116(5)
c (Å)		5.99263(3)	5.94118(4)	5.8979(3)	5.6889(4)	5.509(1)
β (deg)					89.777(4)	89.21(2)
Volume (Å^3)		86.457(1)	171.334(1)	168.984(7)	77.876(8)	72.53(2)
Fe	*z*				0.0009(2)	0.0028(2)
	B_{iso} (Å^2)			0.47(7)	0.40(45)	0.50(5)
	B_{11} (Å^2)	0.85(2)	0.20(4)			
	B_{22}(Å^2)		0.26(4)			
	B_{33}(Å^2)	1.90(8)	0.52(5)			
Se/Te	*z*	0.27388(9)	0.27274(8)	0.2726(5)	0.2867(2)	0.2943(2)
	B_{iso} (Å^2)			0.17(2)	0.10(3)	0.27(8)
	B_{11} (Å^2)	0.97(2)	0.22(2)			
	B_{22} (Å^2)		0.17(2)			
	B_{33} (Å^2)	2.72(6)	1.36(5)			
	Occ. (Se)	0.569(6)	0.574(4)	0.57	0.57	0.57
	Occ. (Te)	0.431(6)	0.426(4)	0.43	0.43	0.43
Fe(2)	*z*	0.696(6)	0.704(5)	0.704	0.731	0.755
	Occ.	0.032(2)	0.030(1)	0.031	0.031	0.031
R_{wp} (%)		7.47%	5.19%	3.03%	1.88%	2.07%
R_{exp} (%)		5.38%	4.44%	1.45%	1.64%	1.99%
Fe-Fe (Å)		2.68753(1) ×4	2.68263(1) ×2	2.6726(1) ×2	2.6162(1) ×2	2.5658(2) ×2
			2.68751(1) ×2	2.6795(1) ×2	2.6163(1) ×2	2.5665(3) ×2
Fe-Se/Te (Å)		2.5110(4) ×4	2.4961(4) ×4	2.483(3) ×4	2.457(3) ×1	2.413(7) ×1
					2.466(3) ×2	2.437(6) ×2
					2.471(4) ×1	2.446(7) ×1
Se/Te-Fe-Se/Te (deg)		115.29(1) ×4	114.99(1) ×2	114.89(9) ×2	116.00(8) ×2	116.61(8) ×2
			114.86(1) ×2	114.70(9) ×2	115.80(8) ×2	116.11(8) ×2
		98.37(2) ×2	99.04(2) ×2	99.3(2) ×2	97.5(2) ×1	97.3(3) ×1
					97.0(2) ×1	95.6(3) ×1

[a] Estimated errors in the last digits are given in parentheses. The positional parameters of the atoms are as follows: space group *P4/nmm*, Fe on 2*a* ($^3/_4$, $^1/_4$, 0), Se/Te and Fe(2) on 2*c* ($^1/_4$, $^1/_4$, *z*); space group *Cmma*, Fe on 4*a* ($^1/_4$, 0, 0), Se/Te and Fe(2) on 4*g* (0, $^1/_4$, *z*); space group $P2_1/m$, Fe on 2*e* ($x \approx {}^3/_4$, $^1/_4$, *z*), Se/Te and Fe(2) on 2*e* ($x \approx {}^1/_4$, $^1/_4$, *z*).

Å; space group *P4/nmm*) of the PbO structural type (Figure 2a) adopted by the $Fe_{1+\delta}Se$ and $Fe_{1+\delta}Te$ end members. Additional weak peaks were also evident in the profile, and these could be accounted for by the presence of a minority hexagonal β-polymorph (space group $P6_3/mmc$, 9.2(1)% fraction). Refinement of the Se/Te content of the sample led to values of 0.569(6)/0.431(6). A search for the location of any excess intercalated Fe proved a difficult task. This is consistent with the presence of only a tiny fraction of such defects in analogy with the isostructural $Fe_{1+\delta}Se$ phase[8] and in contrast to the $Fe_{1+\delta}Te$ end member.[17,18] A difference Fourier analysis of the diffraction data revealed the existence of scattered intensity in the vicinity of the 2*c* ($^1/_4$, $^1/_4$, $z \approx 0.7$) sites in the orthorhombic unit cell. Thus the Rietveld refinements were repeated after introducing an Fe atom in these sites and allowing for its occupation number to vary. This converged to 0.032(2) per formula unit (agreement factors: $R_{wp} = 7.47\%$, $R_{exp} = 5.28\%$, Figure 3S, Table 1).

The evolution of the diffraction profiles on cooling reveals that while the tetragonal structure is initially robust, the response of the *a* and *c* lattice constants is considerably anisotropic (Figure 3). We find that the interlayer spacing contracts normally at a rate, $d\ln c/dT$, of ~32 ppm K^{-1}. However, the basal plane dimensions remain essentially unchanged over a broad temperature range and begin to increase slightly below 100 K. Moreover, as the sample is cooled further, the (*hkl*) ($h,k \neq 0$) reflections in the diffraction profiles begin first to broaden before splitting below $T_s \approx 40$ K (Figure 4 inset), thereby signifying the onset of a structural transformation of the high-temperature tetragonal structure before the onset of superconductivity. Rietveld refinement of the 5 K diffraction profile confirms the

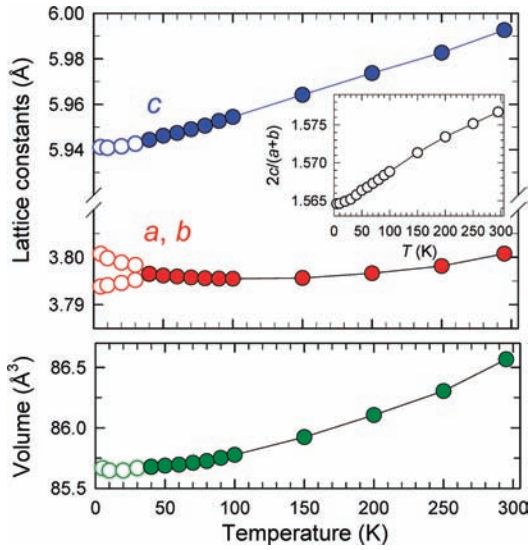

Figure 3. Temperature evolution of the lattice constants (top) and the unit cell volume, V (bottom), in α-$Fe_{1.03}Se_{0.57}Te_{0.43}$. The *inset* shows the temperature dependence of the $2c/(a + b)$ ratio. a and b are divided by $\sqrt{2}$ and V by 2 at temperatures below the tetragonal-to-orthorhombic phase transition at 40 K.

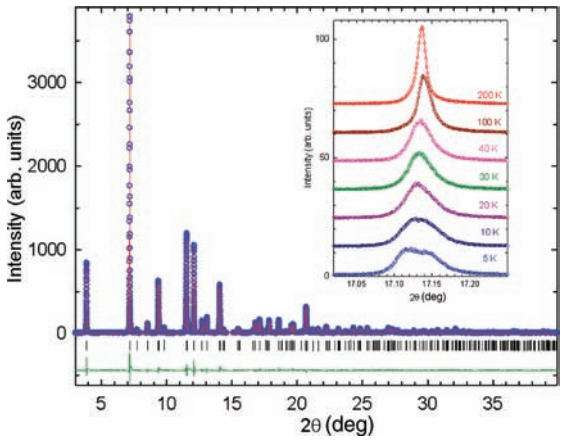

Figure 4. Final observed (blue circles) and calculated (red solid line) synchrotron X-ray (λ = 0.399 88 Å) powder diffraction profile for the α-$Fe_{1.03}Se_{0.57}Te_{0.43}$ sample at 5 K. The lower green solid line shows the difference profile, and the tick marks show the reflection positions. Some peaks arising from the β-polymorph were excluded from the refinement. *Inset*: Temperature dependence of the $(220)_T$ Bragg reflection which on cooling splits into the $[(040)_O, (400)_O]$ doublet below 40 K.

adoption of the same orthorhombic (O) superstructure of lattice dimensions $b_O \approx a_O \approx a_T\sqrt{2}$ and $c_O \approx c_T$ (space group *Cmma*), found before in the parent FeSe system.[9] The refinement results at 5 K are shown in Figure 4 and Table 1 (a_O = 5.37501(3) Å, b_O = 5.36526(3) Å, c_O = 5.94118(4) Å; R_{wp} = 5.19%, R_{exp} = 4.44%) and reveal the development of an extremely small orthorhombic strain, $s = (a - b)/(a + b) = 9 \times 10^{-4}$. With the higher resolution available here, we are able to identify the low-temperature orthorhombic distortion undetectable in previous lower resolution neutron studies.[17] Neither the lattice constant c nor the normalized unit-cell volume V shows a discontinuity at T_s (Figure 3).

Structural Response of α-$Fe_{1.03}Se_{0.57}Te_{0.43}$ to Pressure at Low Temperature. Synchrotron X-ray powder diffraction profiles were collected at 14 K and at pressures between 0.2 and 9.8 GPa. The patterns could be indexed with an orthorhombic cell up to a pressure of 2.0 GPa. The same orthorhombic model (space group *Cmma*) of the α-$Fe_{1.03}Se_{0.57}Te_{0.43}$ structure that we used at ambient pressure was successfully employed in the refinement of these data sets. The Rietveld refinements (2θ range = 3°−27°) proceeded smoothly (Figure 5a, Table 1), revealing a monotonic decrease in the lattice constants and unit cell volume with increasing P (at 2.0 GPa: a_O = 5.2774(4) Å, b_O = 5.2697(4) Å, and c_O = 5.7630(5) Å; agreement factors: R_{wp} = 3.72%, R_{exp} = 1.51%). The response of the lattice metrics to pressure is again strongly anisotropic with the interlayer spacing showing a significantly larger contraction (∼0.013 GPa^{-1}) than the basal plane dimensions (∼0.007 GPa^{-1}) in this pressure range (Figure 6). As the applied pressure increases, the $2c/(a + b)$ ratio decreases rapidly approaching a value of 1.09 at 2.0 GPa.

A further increase in pressure above 2.0 GPa leads to an even higher compression of the $Fe_{1.03}Se_{0.57}Te_{0.43}$ interlayer spacing. However, attempts to employ the same orthorhombic structural model in the refinements proved unsatisfactory, and a progressive worsening of the quality of the Rietveld fits with increasing pressurization was observed. Unlike the case of the parent FeSe material, which shows an $\alpha \rightarrow \beta$ structural phase transition at high pressure,[15] the tetrahedrally coordinated metal α-$Fe_{1.03}Se_{0.57}Te_{0.43}$ phase is found to be robust with no decrease in its fraction observed with increasing P. Instead the most apparent signature of the subtle structural transformation that occurs at 3.0 GPa and above is the inability of an orthogonal metric symmetry structural model to account satisfactorily for the position of the low-angle (001) reflection, thereby necessitating a reduction in symmetry to monoclinic. The high-P diffraction data are necessarily of lower statistical quality than those at ambient P, but they still make clear that all Bragg reflections can be indexed with the monoclinic space group $P2_1/m$, used before to describe the crystal structure of the $Fe_{1.08}Te$ end phase at ambient pressure and low temperature.[17,18] Rietveld refinements employing this structural model gave satisfactory results for all diffraction data sets to the highest pressure of the present experiments at 9.8 GPa (Figure 5a and 5b, Table 1). The structural phase transition at ∼3 GPa is accompanied by a sharp discontinuity in the pressure evolution of the $2c/(a + b)$ ratio with the monoclinic angle, β, monotonically decreasing below 90° with increasing P (Figure 6).

Figure 6 shows the pressure evolution of the unit cell volume of α-$Fe_{1.03}Se_{0.57}Te_{0.43}$ together with a least-squares fit of its 14 K equation of state (EOS) for the high pressure monoclinic phase to the semiempirical third-order Birch−Murnaghan equation:[23]

$$P = \frac{3}{2}K_0[(V_0/V)^{7/3} - (V_0/V)^{5/3}]\left[1 - \frac{3}{4}(4 - K_0')[(V_0/V)^{2/3} - 1]\right] \quad (1)$$

where K_0 is the atmospheric pressure isothermal bulk modulus, K_0' is its pressure derivative (= dK_0/dP), and V_0 is the unit cell volume at zero pressure. The fit results in values of K_0 = 36.6(6) GPa and K_0' = 7.8(3). The extracted value of the volume compressibility, $\kappa = d\ln V/dP$ = 0.027(1) GPa^{-1}, implies a soft compressible solid with a comparable pressure response to that of α-FeSe.[15] We also described the 14 K pressure dependence of each lattice constant with a variant of eq 1, in which K_0 and its pressure derivative, K_0' were substituted by the individual

(23) (a) Birch, F. *Phys. Rev.* **1947**, *71*, 809. Angel, R. J. *Rev. Min. Geochem.* **2000**, *41*, 35.

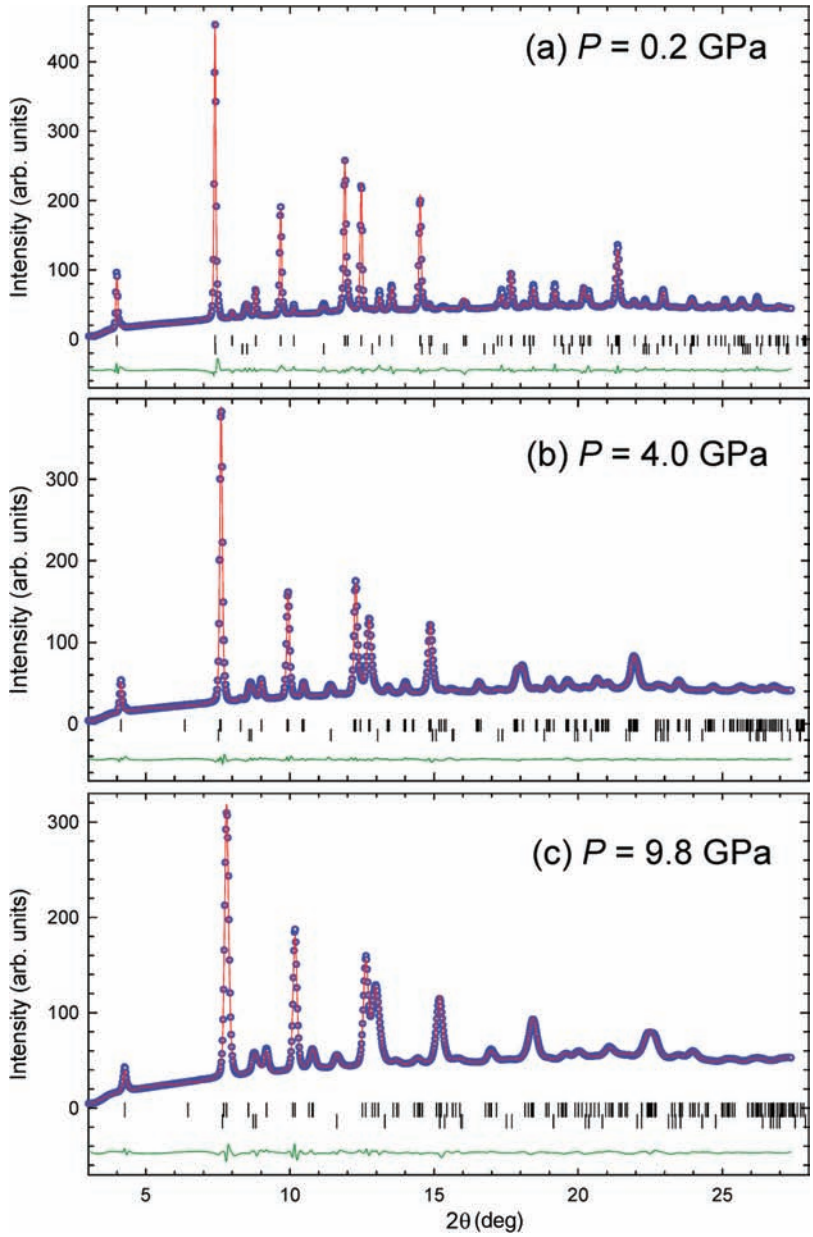

Figure 5. Final observed (blue circles) and calculated (red solid line) synchrotron X-ray ($\lambda = 0.411\ 18$ Å) powder diffraction profile for the $Fe_{1.03}Se_{0.57}Te_{0.43}$ sample at 14 K: (a) 0.2 GPa, (b) 4.0 GPa, (c) 9.8 GPa. The lower green solid line shows the difference profile, and the tick marks show the reflection positions of the α- (upper) and β- (lower) phases, respectively.

K_x and K_x' ($x = a, b, c$) values. The results of these fits for data above 3 GPa are also included in Figure 6 and give the following: $K_a = 42(1)$ GPa, $K_a' = 15.3(9)$; $K_b = 54.3(8)$ GPa, $K_b' = 4.6(3)$; $K_c = 22.8(5)$ GPa, $K_c' = 6.9(3)$. These values clearly reveal the diversity in bonding interactions present, with the solid being least compressible in the basal plane *ab*, in which the covalent Fe−Se/Te bonds lie ($d\ln a/dP = 0.024(1)$ GPa^{-1}, $d\ln b/dP = 0.018(1)$ GPa^{-1}). The interlayer compressibility, $d\ln c/dP = 0.044(1)$ GPa^{-1}, is ∼2 times larger, consistent with the very soft Se/Te−Se/Te interlayer interactions.

Discussion

The most apparent structural characteristic of the family of $Fe_{1+\delta}Se_{1-x}Te_x$ superconductors is their relative structural simplicity when compared to their isostructural iron arsenide analogues, which allows ready identification of the relationship between key structural features generically present in all of the Fe-based superconductors and T_c. The absence of interleaved cations or rare-earth oxide slabs allows close proximity of the electronically active $Fe_2(Se/Te)_2$ layers, potentially rendering the electronic structures more three-dimensional. For instance, in the FeSe binary, the ∼2.91-Å Fe_2Se_2 layers are separated by only ∼2.58 Å. Partial substitution of Se by the larger Te atoms in $Fe_{1.03}Se_{0.57}Te_{0.43}$ naturally leads to both an increased $Fe_2(Se/Te)_2$ slab thickness (∼3.28 Å) and an increased interslab separation of ∼2.71 Å at 295 K. Nonetheless the separation between the layers is still significantly smaller than that found in the iron arsenide families where it ranges from 3.34 Å in LiFeAs to 5.79 Å in SmFeAsO.[5,11]

The geometry of the $FePn_4$ tetrahedral units has been identified as a possible control parameter of T_c in the iron pnictides, and it has been argued that it sensitively controls the width of the electronic conduction band. The magnitude of the Pn−Fe−Pn angles was empirically found as the important

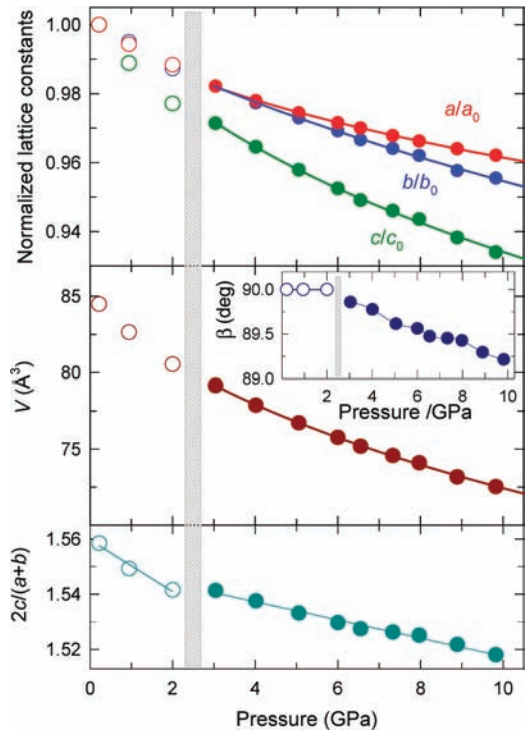

Figure 6. Pressure evolution of the normalized lattice constants (top), the unit cell volume, V (middle), and the $2c/(a + b)$ ratio (bottom) at 14 K in α-$Fe_{1.03}Se_{0.57}Te_{0.43}$. The *inset* shows the temperature dependence of the monoclinic angle β. a and b are divided by $\sqrt{2}$ and V by 2 at temperatures below the orthorhombic-to-monoclinic phase transition (shaded region) at 3 GPa.

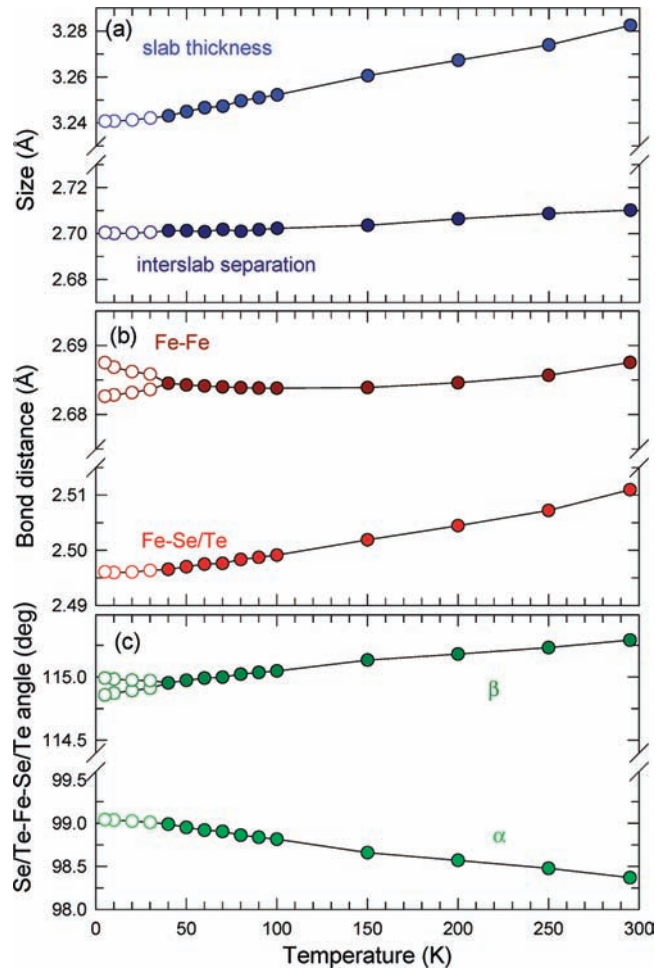

Figure 7. Temperature evolution of selected bond distances and angles in α-$Fe_{1.03}Se_{0.57}Te_{0.43}$ at ambient pressure. (a) $Fe_2(Se/Te)_2$ slab thickness and interslab separation. (b) Fe−Fe and Fe−Se/Te distances. (c) Se/Te−Fe−Se/Te bond angles (dark green circles, angle β bisected by the basal plane; light green circles, angle α bisected by the c axis). Open symbols denote the values of the crystallographic parameters below the tetragonal-to-orthorhombic phase transition at 40 K.

parameter in tuning the electronic properties of these systems and therefore determining T_c, which is maximized when the $FePn_4$ units are close to regular with all Pn−Fe−Pn angles near 109.47°.[24] The $Fe(Se/Te)_4$ tetrahedra in $Fe_{1.03}Se_{0.57}Te_{0.43}$ are highly compressed in the basal plane; at 295 K, the Se/Te−Fe−Se/Te angle which is bisected by the c axis is 98.4°, while the Se/Te−Fe−Se/Te angle which is bisected by the ab plane is 115.3°, a difference of 16.9°. This results in an even more strongly distorted shape of the tetrahedra than that found in the FeSe end member where this angle difference is considerably smaller at 7.5°. As $Fe_{1.03}Se_{0.57}Te_{0.43}$ has a higher T_c than FeSe, the above empirical conjecture[24] is clearly violated in the case of the iron chalcogenide superconductors. Alternatively, the height of the pnictogen atoms above the iron plane, h_{Pn} (*i.e.*, half the slab thickness), has been also identified as sensitively controlling T_c in the iron pnictides.[25] We note here that $h_{Se/Te}(Fe_{1.03}Se_{0.57}Te_{0.43}) = 1.64$ Å $> h_{Se}(FeSe) = 1.455$ Å at 295 K and ambient P, and at first sight, this is consistent with the relative magnitudes of the superconducting transitions; however, a more stringent test of this theoretical model is provided by the high-P structural data which will be discussed below.

The basal plane dimensions of the high-temperature tetragonal phase of $Fe_{1.03}Se_{0.57}Te_{0.43}$ also show an unusual behavior with a change in temperature. The thermal expansivity in the 295 to 100 K temperature range is extremely small at ~7 ppm K^{-1} (this is also tracked by the response of the Fe−Fe distances) and contrasts sharply with the behavior of the c axis which shows an expansivity 4 times as large in the same temperature range (Figure 3). Moreover, on further cooling below 100 K the thermal expansivity of the basal plane changes sign and the size increases (Figure 3). These experimental observations can be understood by referring to Figure 7 which summarizes the temperature evolution of selected bond distances and angles in $Fe_{1.03}Se_{0.57}Te_{0.43}$. Two competing geometrical effects on the response to temperature of the size and shape of the edge-sharing $Fe(Se/Te)_4$ tetrahedra can be identified. First, the Fe−Se/Te bond distances decrease continuously on cooling, leading to normal thermal contraction of the basal plane. However, at the same time, the temperature dependence of the Se/Te−Fe−Se/Te bond angles is such that a progressively decreasing tetrahedral distortion results; this leads to a gradual relief of the tetrahedral compression in the basal plane and, therefore, to a size inflation of the ab plane and a size contraction in the c direction. This latter effect can also account for the larger decrease in the $Fe_2(Se/Te)_2$ slab thickness compared to that of the interslab separation in this temperature range (Figure 7).

(24) Lee, C.-H.; Iyo, A.; Eisaki, H.; Kito, H.; Fernandez-Diaz, M. T.; Ito, T.; Kihou, K.; Matsuhata, H.; Braden, M.; Yamada, K. *J. Phys. Soc. Jpn.* **2008**, *77*, 083704.
(25) Kuroki, K.; Usui, H.; Onari, S.; Arita, R.; Aoki, H. *Phys. Rev. B* **2009**, *79*, 224511.

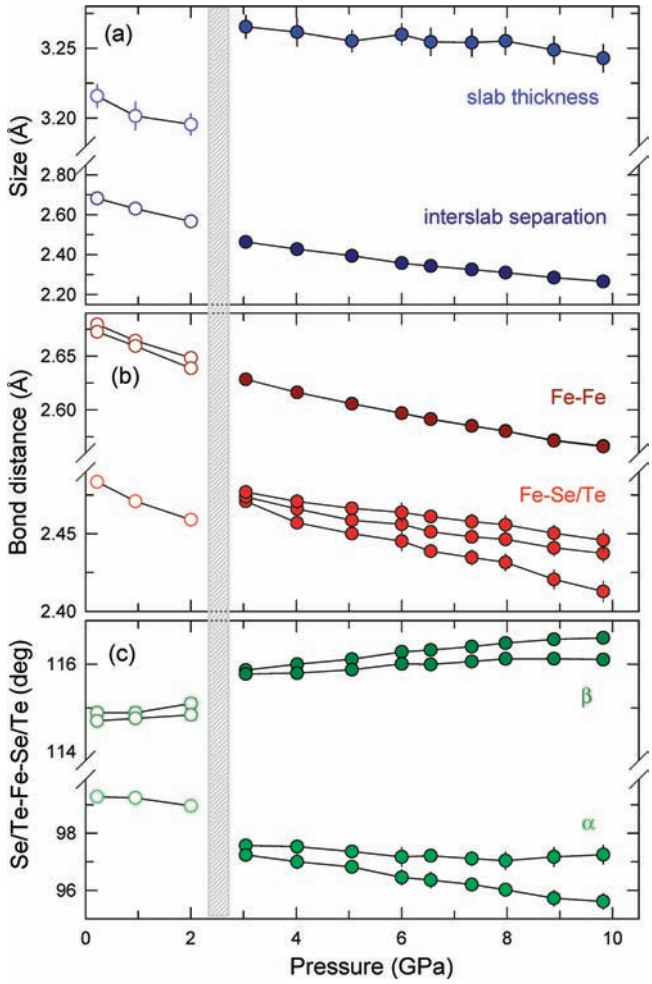

Figure 8. Pressure evolution of selected bond distances and angles in α-$Fe_{1.03}Se_{0.57}Te_{0.43}$ at 14 K. (a) $Fe_2(Se/Te)_2$ slab thickness and interslab separation. (b) Fe−Fe and Fe−Se/Te distances. (c) Se/Te−Fe−Se/Te bond angles (dark green circles, angle β bisected by the basal plane; light green circles, angle α bisected by the *c* axis). Open symbols denote the values of the structural parameters below the orthorhombic-to-monoclinic phase transition (shaded region) at 3 GPa.

Another important point arising from the temperature-dependent ambient *P* synchrotron X-ray data is that the superconducting $Fe_{1.03}Se_{0.57}Te_{0.43}$ phase is also metrically orthorhombic and isostructural with the superconducting FeSe end member, while nonsuperconducting $Fe_{1+\delta}Se$ compositions lack a structural distortion away from tetragonal at low temperatures.[26] However, the influence of the T → O phase transition on the local geometry of the edge-sharing $Fe(Se/Te)_4$ tetrahedra is only extremely subtle (Table 1) and its consequences for the electronic structure still remain to be understood; at high *T*, there is a single Fe−Fe distance (at 295 K: 2.6875 Å), and below T_s, there are two symmetry-inequivalent Fe−Fe distances (at 5 K: 2.6826 and 2.6875 Å). This bond alternation (∼0.005 Å) is smaller than that found in superconducting FeSe (∼0.013 Å). Similarly, one set of the Se/Te−Fe−Se/Te angles remains unaltered (at 295 K, 98.4°; at 5 K, 99.0°), while the second set (at 295 K, 115.3°) splits into two (at 5 K, 115.0° and 114.9°). On the other hand, the twisting of the tetrahedra at low temperatures does not affect the Fe−Se/Te bonds, and there is a single distance in both the tetragonal and orthorhombic phases (at 295 K, 2.511 Å; at 5 K, 2.496 Å).

The low-temperature structural response to *P* of orthorhombic $Fe_{1.03}Se_{0.57}Te_{0.43}$ is distinctly different from that of the isostructural parent FeSe. The partial introduction of the larger Te atom extends the stability range of the layered α-phase to the highest *P* of the present experiments (∼10 GPa) in sharp contrast to the behavior of α-FeSe which upon pressurization converts near 9 GPa to the more densely packed NiAs-structured β-polymorph with an accompanying volume collapse and a change of the Fe−Se coordination from tetrahedral to octahedral.[15,16] The origin of the differing behavior may be associated with the retention of significantly larger interlayer separations for $Fe_{1.03}Se_{0.57}Te_{0.43}$ in the same pressure range (Se/Te−Se/Te interlayer contacts ∼3.42 Å at 9.8 GPa) and the disfavoring of the higher coordination number in the β-phase by the larger Te ligand. In addition, while FeSe remains strictly orthorhombic until the onset of the α→β phase transformation, here we find that $Fe_{1.03}Se_{0.57}Te_{0.43}$ shows a phase transition to a monoclinic structure at a relatively low pressure of ∼3 GPa. Presumably the ability to undergo this distortion also stabilizes the layered $Fe_{1.03}Se_{0.57}Te_{0.43}$ phase against the more drastic transformation to the β-polymorph at higher *P*. The orthorhombic-to-monoclinic crystal symmetry crossover is remarkably coincident with a change in the electronic properties of the material, as evidenced by the switch of the pressure coefficient of T_c, dT_c/dP, from positive (orthorhombic phase) to negative (monoclinic phase) (Figure 1c). As a result, the onset of the structural transition occurs at the same pressure at which T_c is found to be maximum (23.3 K at 2.3 GPa). Superconductivity with monotonically decreasing T_c survives in the monoclinic phase to very high pressures until 11.9 GPa, at which point it is completely suppressed. Notably $Fe_{1.03}Se_{0.57}Te_{0.43}$ remains metallic following the disappearance of the superconducting response.

The effect of pressure on the local geometry of the $Fe(Se/Te)_4$ tetrahedra in orthorhombic $Fe_{1.03}Se_{0.57}Te_{0.43}$ is analogous to that observed in isostructural FeSe.[15] The height of the chalcogen atoms above the basal plane decreases monotonically with increasing *P* (Figure 8a), while at the same time the edge-sharing tetrahedral units become even more distorted and their compression in the basal plane increases (Figure 8c). At the same time, superconducting T_c increases monotonically with pressure in both FeSe and $Fe_{1.03}Se_{0.57}Te_{0.43}$ in sharp contrast to the theoretical expectations[24,25] that T_c should be maximal for tetrahedral regularity and for large iron-chalcogen slab thicknesses. This discrepancy remains to be understood especially as the situation may be further complicated by pressure tuning of the effective doping level as the interlayer Se/Te−Se/Te interactions change. However, it appears that, in the orthorhombic superconducting phases, higher T_c's are promoted by smaller interlayer spacings (increased dimensionality).

Above 3 GPa, the superconducting $Fe_{1.03}Se_{0.57}Te_{0.43}$ phase becomes metrically monoclinic and the phase transition is accompanied by subtle but well-defined discontinuities in the $2c/(a+b)$ ratio (Figure 6) and in various structural parameters (Figure 8). There is a clear increase in the Fe−Se/Te bond lengths which in combination with the smooth decrease in the Fe−Fe bond lengths (Figure 8b) leads to an inflation in the size of the $Fe_2(Se/Te)_2$ slab thickness (Figure 8a). At the same time, the distortion of the $Fe(Se/Te)_4$ tetrahedra away from regularity sharply increases (Figure 8c). A principal influence of the O → M transition is on the regularity of the Fe−Se/Te tetrahedral bonding; at low *P*, there is a single Fe−Se/Te bond distance

(26) McQueen, T. M.; Williams, A. J.; Stephens, P. W.; Tao, J.; Zhu, Y.; Ksenofontov, V.; Casper, F.; Felser, C.; Cava, R. J. *Phys. Rev. Lett.* **2009**, *103*, 057002.

(at 2.0 GPa: 2.46 Å), and above P_s, there are three symmetry inequivalent Fe−Se/Te distances whose difference in magnitude increases with increasing P (at 9.8 GPa, 2.41, 2.44, and 2.45 Å). Similarly, there are four symmetry-inequivalent Se/Te−Fe−Se/Te angles in the high pressure monoclinic phase. On the other hand, although there are still two inequivalent Fe−Fe distances present at high P, the very small Fe−Fe bond alternation of the low P orthorhombic phase appears to be removed. Overall the effect of increasing P is to increase the monoclinic lattice distortion (the monoclinic angle β decreases monotonically below 90°) and the irregularity in shape and bonding of the $Fe(Se/Te)_4$ building blocks. In particular, the change from a single Fe−Se/Te distance to multiple distances is the most pronounced structural difference and, unlike the benign effect on T_c of the enhanced angular distortion with increasing P seen in the orthorhombic FeSe and $Fe_{1.03}Se_{0.57}Te_{0.43}$ phases, suppresses T_c.

The most prominent point arising from our structural and resistivity results as a function of pressure is that the maximum in the T_c *vs* P superconducting dome at ∼2.3 GPa coincides exactly with the crossover from orthorhombic ($P \leq 2.0$ GPa) to monoclinic ($P \geq 3.0$ GPa) crystal symmetry (Figure 1c). This unambiguously points toward the crucial role played by the structural order in determining the bonding interactions within the conducting $Fe_2(Se/Te)_2$ slabs and the electronic properties of the $Fe_{1+\delta}Se_{1-x}Te_x$ superconductors; the symmetry as well as carrier concentration and bond lengths must be right in order to optimize T_c. In this context, the orthorhombically distorted *Cmma* phase emerges as the optimal phase to achieve high T_c in this family of materials with both raising and lowering the symmetry suppressing T_c; nonsuperconducting compositions of $Fe_{1+\delta}Se$ are tetragonal,[26] and monoclinic symmetry is detrimental to superconductivity in $Fe_{1+\delta}Se_{0.57}Te_{0.43}$. Attempts to raise the T_c of the iron chalcogenides beyond its current maximum of 37 K (observed for α-FeSe at ∼7 GPa)[15,16] should therefore aim to stabilize orthorhombic crystal symmetry at as high an applied pressure as possible by suppressing both the pressure-induced competing α → β and orthorhombic → monoclinic structural instabilities.

Conclusions

In conclusion, we have presented synchrotron X-ray powder diffraction structural measurements on the ternary α-$Fe_{1.03}Se_{0.57}Te_{0.43}$ superconductor ($T_c = 13.9$ K at ambient P) at both ambient and elevated pressures. We have found that at low temperatures ($T_s = 40$ K) it adopts an orthorhombic superstructure of the high-temperature tetragonal anti-PbO-type layered structure. In contrast to the isostructural α-$Fe_{1+\delta}Se$ end member, the layered structure is robust at low temperatures to the application of pressure as high as 10 GPa and does not transform to the nonsuperconducting hexagonal NiAs-structured β-polymorph. However, above 3 GPa, we identify the occurrence of a structural phase transition to a phase with monoclinic symmetry. The pressure onset of this transformation coincides exactly with the maximum superconducting T_c of 23.3 K at 2.3 GPa (established by complementary pressure-dependent resistance measurements), revealing that crystal symmetry and electronic properties are closely linked; T_c increases with increasing P for the orthorhombic phase, but the trend is sharply reversed and T_c decreases with increasing P for the monoclinic phase until at ∼12 GPa a metallic but not superconducting state is observed.

Acknowledgment. We thank the ESRF and SPring-8 for provision of synchrotron X-ray beamtime, EPSRC for support (MJR, EP/C511794), and A. N. Fitch (ESRF) for help with the experiments.

Supporting Information Available: Pressure dependence of the shielding fraction, temperature dependence of the resistance near T_c, and Rietveld refinement of the diffraction profile at ambient temperature and pressure. This material is available free of charge via the Internet at http://pubs.acs.org.

JA907345X